Nonlinear FEM–BEM Formulation and Model-Free Inversion Procedure for Reconstruction of Cracks Using Pulse Eddy Currents

Gabriel Preda, Bogdan Cranganu-Cretu, Florea Ioan Hantila, Ovidiu Mihalache, Zhenmao Chen, and Kenzo Miya

***Abstract*—Pulse eddy currents are proposed as a nondestructive testing (NDT) technique to detect flaws in conductive structures with large thickness. The harmonic component of a pulse is rich, the pick-up signal containing the amount of information corresponding to multifrequency analysis. Due to the short time length of the pulse, the amplitude of the excitation increases up to 100 times of the amplitude for an ac signal. Both direct simulation of pulse eddy-currents phenomena using an A-ϕ FEM–BEM code and neural networks-based inversion techniques are performed. Numerical results for the inversion of signals due to outer defects are shown.**

***Index Terms*—Eddy-current testing, neural networks, nonlinear media.**

I. Introduction

EDDY-CURRENT testing (ECT) using sinusoidal mode has been extensively used for detection of flaws in metallic structures such as steam generator (SG) tubing in pressurized water reactor (PWR) power plants. Despite its advantages as high speed and reliability to in-service inspection, this method is limited by skin effect only to thin, nonmagnetic structural components. A possible alternative is the use of pulse eddy currents. This option provides a multifold advantage: the rich harmonic component of a pulse accounts for a multifrequency analysis, the lower harmonics penetrating deeper in the structure, while the short duration of a signal allows an increase in the power for the same heating exposure of the coil-probe system [1], [2]. Besides this, by exposing a ferromagnetic material to a high-power pulse, the instant magnetic saturation increases the penetration depth of eddy currents, by attenuating the double negative effect of frequency-times-permeability-times-conductivity term that appears in eddy-current skin-depth computation and the air–iron interface condition, allowing the inspection of structures with large thickness [3]. Various industrial applications were reported, such as detection of cracks in multilayered plates around fasteners in aeronautics industry [4], thickness and conductivity evaluation and crack detection, and sizing in structural steels [3]. The present study illustrates the possibility of crack shape reconstruction using simulated pulse eddy-current signals. The applied inverse procedure uses neural networks and additional regularization methods as *shifting aperture* and principal component analysis (PCA) [5].

Manuscript received July 5, 2001; revised October 25, 2001.

G. Preda was with the School of Engineering, the University of Tokyo, Japan. He is now with the International Institute of Universality, Tokyo 113–0031, Japan, on leave from "Politechnica" University of Bucharest, Bucharest 77206, Romania (e-mail: preda@jsaem.gr.jp).

B. Cranganu-Cretu was with JSAEM, Tokyo, Japan. He is now with the International Institute of Universality, Tokyo 113–0031, Japan, on leave from "Politechnica" University of Bucharest, Bucarest 77206, Romania (e-mail: bogdan@jsaem.gr.jp).

F. I. Hantila is with the Department of Electrical Engineering, "Politehnica" University of Bucharest, Bucharest 77206, Romania (e-mail: hantila@elth.pub.ro).

O. Mihalache was with the School of Engineering, the University of Tokyo, Japan. He is now with the Japan Nuclear Cycle Development Institute, Tsuruga 914-8585, Japan.

Z. Chen was with JSAEM, Tokyo, Japan. He is now with the International Institute of Universality, Tokyo 113-0031, Japan (e-mail: chen@jsaem.gr.jp).

K. Miya was with the School of Engineering, University of Tokyo, Japan. He is now with the International Institute of Universality, Tokyo 113-0031, Japan (e-mail: miya@jsaem.gr.jp).

Publisher Item Identifier S 0018-9464(02)01257-8.

II. Numerical Formulation for the Forward Problem

A three-dimensional (3-D) finite-element–boundary-element method (FEM–BEM) coupling, based on A-ϕ formulation for transient nonlinear eddy currents was developed. From Maxwell equations in the limit of quasi-stationary field, taking into account the constitutive relationships

$$\mathbf{H} = \mathbf{F}(\mathbf{B}) \tag{1}$$

$$\mathbf{J} = \sigma \mathbf{E} \tag{2}$$

and using the Coulomb gauge $\nabla \cdot \mathbf{A} = 0$, the governing equations are obtained

$$-\frac{1}{\mu_0}\Delta\mathbf{A} + \sigma\left(\frac{\partial \mathbf{A}}{\partial t} + \nabla\frac{\partial \phi}{\partial t}\right) = \nabla \times \mathbf{M} \qquad \text{in } \Omega_c \tag{3}$$

$$\nabla \cdot \sigma\left(\frac{\partial \mathbf{A}}{\partial t} + \nabla\frac{\partial \phi}{\partial t}\right) = 0 \qquad \text{in } \Omega_c \tag{4}$$

$$-\frac{1}{\mu_0}\Delta\mathbf{A} = \mathbf{J}_0 \qquad \text{in } \Omega_0 \tag{5}$$

where

Ω $= \Omega_c \cup \Omega_0$ whole space;
Ω_c conductive domain including ferromagnetic parts;
Ω_0 air.

The field sources are the impressed current sources $\mathbf{J}_0$ in the air and the magnetization inside the ferromagnetic domains. The nonlinear media having the constitutive relationships (1) are replaced by a linear one having vacuum permeability and a mag-

netization iteratively corrected through a fixed-point procedure based on Polarization method [6]. Equation (1) is replaced by

$$\mathbf{M} = \frac{1}{\mu_0}\mathbf{B} - F(\mathbf{B}) = G(\mathbf{B}). \tag{6}$$

On the interface between FEM-domain (conductive and ferromagnetic) and BEM-domain (air), the tangential component of $\mathbf{H}$ is enforced only in a weak sense [7]

$$\frac{1}{\mu_0}\frac{\partial \mathbf{A}}{\partial \mathbf{n}} - \mathbf{M}\times\mathbf{n}\Big|_{\mathrm{FEM}} = \frac{1}{\mu_0}\frac{\partial \mathbf{A}}{\partial \mathbf{n}}\Big|_{\mathrm{BEM}}. \tag{7}$$

Using Galerkin approach, (3)–(5) are discretized by projecting each term of the equations on the shape functions and integrating over the entire problem domain Ω [8]. The equation system obtained after FEM–BEM coupling using interface condition (7) is

$$[K]\{\mathbf{A}\} + [Q]\begin{Bmatrix} \partial \mathbf{A}/\partial t \\ \partial \phi/\partial t \end{Bmatrix} = [R]\{F_0\} + [S]\{\mathbf{M}\} \tag{8}$$

where K and Q are banded, partially full matrices. A Crank–Nicholson integration scheme with constant time step and $\Theta = 1/2$ (or $\Theta = 1$, for the nonlinear problem) is used and the equivalent nonlinear system is solved every time step

$$[K]\{\theta X_k^i + (1-\theta)X_{k-1}^i\} + [Q]\left\{\frac{X_k^i - X_{k-1}^i}{\Delta t}\right\} = \{F_{Jk}^i\}. \tag{9}$$

All the coefficients in the matrix system and right-hand side terms are unchanged through time integration and nonlinear iterations and, therefore, the resulting matrix system is formed and inverted only once. This results in considerable speed-up of the overall computation process, when large databases for defect reconstructions are built. Each time step, a nonlinear equation is solved, through a fixed-point procedure described extensively elsewhere [6].

The time step is adapted to each particular problem in order to simulate accurately the fast variable regime of pulse eddy currents. The mesh is also subject of a particular attention, the rich harmonic components of a pulse imposing to adapt its size to the smallest skin-depth, corresponding to the larger frequency component to be taken into account.

III. Simulation Setup and Sensitivity Analysis

As first application of the method, only conductive media are taken into account. A pancake coil is used to energize the specimen and a Hall sensor for detecting the z component (orthogonal on the plate surface) of magnetic flux density under the axis of the coil. The system pancake probe-Hall sensor is less sensible to frequency variation than the classic auto-induction pancake used in AC detection [2]. In the case of AC, the pancake probe is optimized for a certain frequency. In the case of pulse eddy-current excitation, due to the rich harmonic component of the signal, such a frequency-optimization technique is hampered.

The simulations were performed for a 50 mm $\times$ 50 mm square, 10 mm thick nonferromagnetic plate, with conductivity

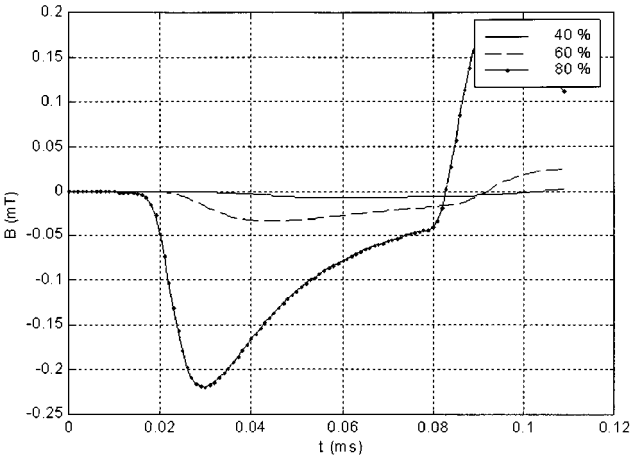

Fig. 1. Difference signals for cracks ranged from 40% to 80% OD, 0.5 mm wide, 7 mm long. The signal is z component of magnetic flux density at 0.5 mm over the 10-mm-wide conductive plate.

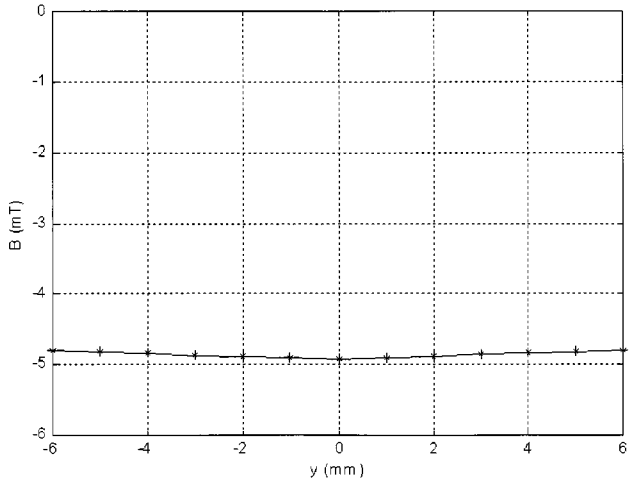

Fig. 2. Pick-up signal obtained by sampling at $t = 40$ μs. The crack is OD 80%, 10 mm long, and 0.5 mm wide.

$\sigma = 10^6$ S/m, using a single pulse with duration 90 μs, with rise and fall time 10 μs (rise and fall exponentially), recurrence frequency 100 Hz and amplitude $I_{\max} = 2500$ AT (100 A/mm^2). The pancake coil has the dimensions: external radius $R_{\max} = 6$ mm, internal radius $R_{\min} = 1$ mm and height $Z = 5$ mm. The coil lift-off is 1 mm, the pick-up sensor lift-off is 0.5 mm. In this simulation, time step is 1 μs; 110 steps were simulated. Scan velocity admitted is 0.1 m/s with a scan pitch of 1 mm. Fig. 1 shows the difference between the signal with crack and the signal without crack (difference signal), as a function of time. We can notice that the maximum amplitude of the difference signal is reached earlier for defects positioned closer to the surface and later for deeper defects. By appropriately selecting the sampling time, we can enhance the sensitivity of the method toward a subclass of defects (for example, delaying the sampling moment, we increase the sensitivity to deeper embedded defects, reducing in the same time the amplitude of the signal). Fig. 2 shows the signal obtained while scanning over an 80% OD crack, 10 mm long, and 0.5 mm wide, between $y = -6$ mm and $y = 6$ mm (13 points with pitch 1 mm), with the sampling moment set at 40 μs.

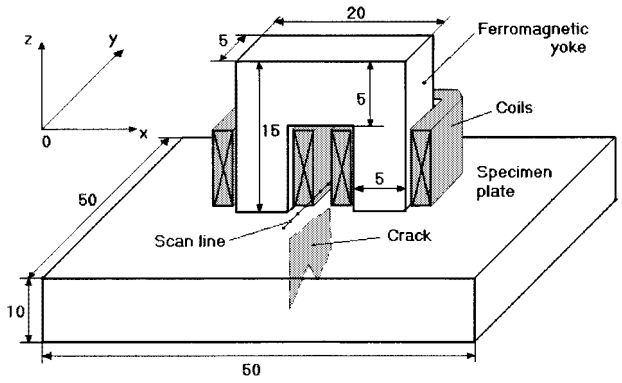

Fig. 3. A plate specimen having $\boldsymbol{B}$–$\boldsymbol{H}$ characteristic of F82H is excited using a yoke made of pure iron. The dimmensions for the plate and yoke are shown in the figure (dimmensions given in millimeters). Two solenoid coils, with total current $I_{\rm tot} = 100$ AT each (current density 2.85 A/mm^2) and with dimensions inner radius $R_{\rm min} = 3.6$ mm, outer radius $R_{\rm max} = 7.1$ mm and height $Z = 10$ mm, are used to energize the yoke. The air gap between yoke and plate is 1 mm and the sensor liftoff is 0.5 mm, the B-scan line is between $y = -5$ and $y = 5$ mm (centered over the plate specimen, along with the crack and under the yoke), with a pitch of 1 mm.

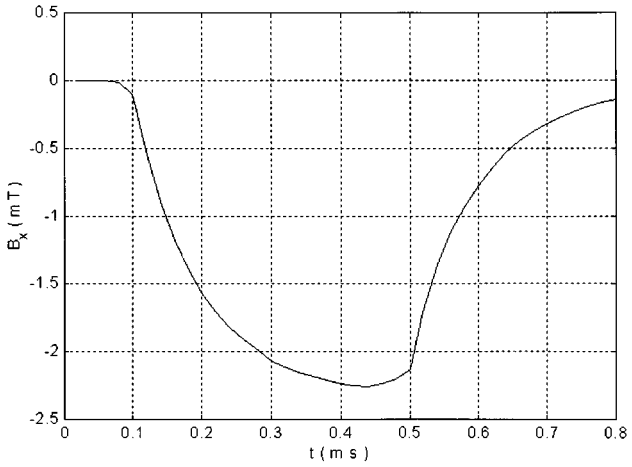

Fig. 4. The x component of magnetic flux density. Signal in the central point of the scan pline, for $y = 0$ mm, at $x = 0$ and $z = 0.5$ mm over the plate.

A second case analyzed includes ferromagnetic materials and a low-frequency pulse excitation. A plate specimen made of ferromagnetic material F82H [9], with dimmensions 50 mm × 50 mm and thickness 10 mm is energized using a yoke made from pure iron (see Fig. 3). The yoke is equiped with two solenoidal coils, with dimensions as follows: external radius $R_{\rm max} = 7.1$ mm, internal radius $R_{\rm min} = 3.6$ mm and height $Z = 10$ mm. The excitation is a trapezoidal-shaped pulse with total duration 0.6 ms, rise and fall exponentially, both having 0.2 ms. The peak value of the total current in each coil is $I_{\rm tot} = 100$ AT (current density is 2.85 A/mm^2). The time step is set to 20 μs, the number of time steps being 40. In Fig. 4, we show the signal variation in time, including the effect due to the eddy currents and magnetization. The difference signals for OD cracks, 7 mm long, 0.5 mm wide, ranged from 20% to 80% deep are shown in Fig. 5, sampled in the central position on y axis. For the same cracks, we show the peak value of each signal for different positions along axis y in Fig. 6.

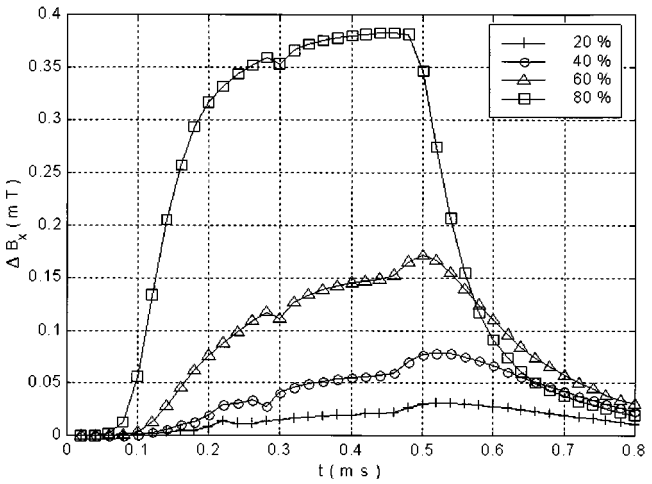

Fig. 5. Comparison between difference signals, for defects 0.5 mm wide, 7 mm long, ranged from 20% to 80% deep; scan point at $x = 0$, $z = 0.5$, $y = 0$ mm.

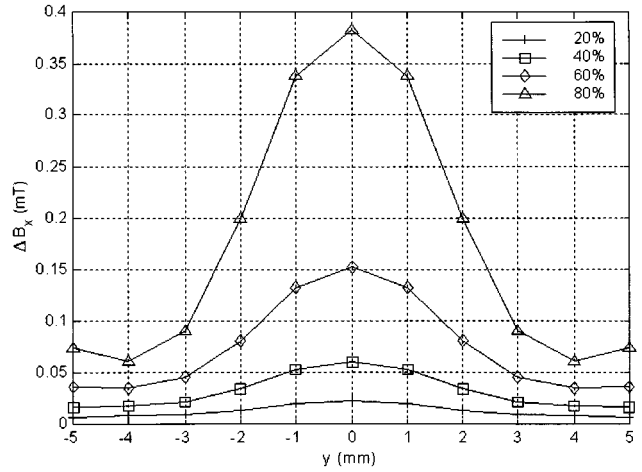

Fig. 6. The x component of magnetic flux density sampled at $t = 0.46$ ms.

IV. Inversion Procedure Using Neural Networks

A *neural network* (NN) is used for reconstruction of crack parameters (output values) from signals of magnetic flux densities (inputs). Additionally, to a statistical analysis and transformation of input data, by *principal component analysis* (PCA), and NN with incrementally learning, a special data fragmentation-data fusion technique is used. The procedure, called *shifting aperture* [5] reduces the ill-posedness of the problem, minimize the network dimensions, and multiply the input data. In each training epoch, one node is added to the single hidden layer of the network. The training algorithm of the employed NN implies the least-squares solution of an over-determined equation system [5], [10], for every iteration (training epoch)

$$[\mathbf{I} \quad f_1(\mathbf{I}\cdot\mathbf{W}_{ih})]\cdot\begin{bmatrix}\mathbf{W}_{io}\\ \mathbf{W}_{ho}\end{bmatrix} = f_2^{-1}(\mathbf{O}) \tag{10}$$

where $\mathbf{I}$, $\mathbf{O}$ represent the input, and output training sets, respectively, f_1 and f_2, the nonlinear activation functions for the hidden and output nodes, $\mathbf{W}_{ih}$ is a randomly generated, fixed

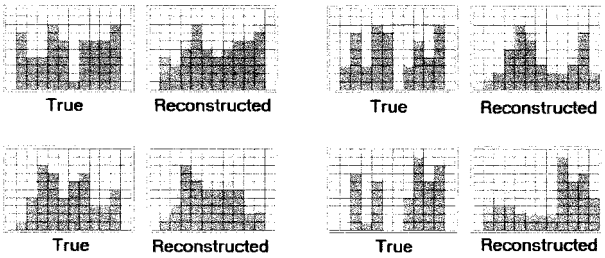

Fig. 7. Reconstruction of OD cracks in the case of conductive plate. Cell dimensions are 1 mm in length and 1 mm in height. Each reconstruction is obtained by a weighted superposition of eight shifted apertures, each cell value being obtained by superposition of one to five windows values. Dark color means crack (0-value) whilst light color means base material (1-value), the blurred areas being associated with reconstructed values in between the two extremes. True profiles are shown in the left side of each reconstructed ones.

coefficient matrix, and $\mathbf{W}_{io}$, $\mathbf{W}_{ho}$ are the matrices containing the unknowns of the problem, i.e., the input–output (I–O) and the hidden- output interconnection weights, respectively.

For the case of the conductive plate excited with pancake-type coil, a database of cracks and corresponding signals was constructed through simulations. The I–O pairs of the initial database are partitioned into training, validation and verification sets. Initially, 250 longitudinal scans were simulated along the same number of inner defects in a plate specimen. Each complete scan consisted of 13 sensor readings along a probing line parallel to the crack mouth, with 1 mm pitch. Apertures of five elements, and estimation windows of six reading points were taken. From the total of 250 complete, 13-points scans, were formed in this way 2000 such I–O vector pairs. For training, 1760 I–O pairs were used, 160 for validation and 80 for verification (test) set. The training was stopped after about 550 epochs, the minimal validation error being obtained at epoch 236. Only unjittered signals were used for training. In Fig. 7, four reconstruction examples are presented in gray-level images, black corresponding to vanished conductivity and white to base material. Each image represents a 12-mm-long profile, which is obtained by a weighted superposition of eight successive windows, each cell value being obtained by superposition of one to five cell values with different weights.

For the second case analyzed here, the ferromagnetic plate excited with a yoke, we prepared a database of signals and crack parameters of 200 cases. Each scan set has 11 points (equally pitched from $y = -5$ to 5 mm, along the y axis), along the crack. The defects are parameterized at a cell level, each cell having 1 mm in length and 2 mm in depth, the crack being 0.5 mm wide.

Only 150 cases were used for the training, 40 for validation and 10 were kept for test. The shifting aperture technique was not used. The training was stopped after 250 steps and the optimum configuration of the network, used then for reconstruction, was achieved at step 85. The results are shown in Fig. 8, and are in good agreement with the true shapes, plotted as well in the same figure.

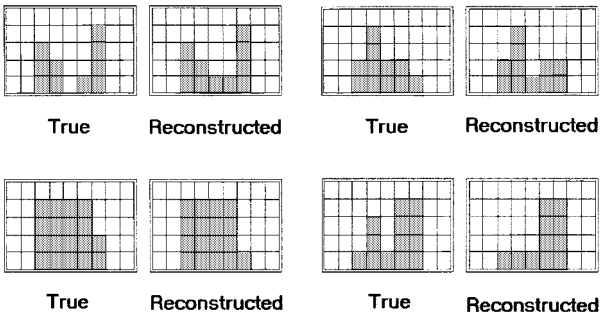

Fig. 8. In the case of ferromagnetic plate (F82H) and excitation with fixed yoke, only the sensor scans in y direction, for sampling the x component of magnetic flux density. From the set of 10 reconstructions we show here four examples. Cell dimensions are 1 mm in length and 2 mm in height. The reconstructed profiles are compared with the original ones, plotted for each case in the left side.

V. Conclusion

The simulations shows that the proposed method, based on application of pulse eddy currents, gives good results for detection of crack in thick conductive or ferromagnetic structures. An inverse procedure, based on NN and various regularization method is used for reconstructing the shape of the cracks from the values of the magnetic flux density signals sampled using a Hall-sensor. The reconstructions agree fairly well with the true crack profiles.

References

[1] J. Bowler and M. Johnson, "Pulsed eddy-current response to a conducting half-space," *IEEE Trans. Magn.*, vol. 33, pp. 2258–2264, May 1997.

[2] M. Gibbs and J. Campbell, "Pulsed eddy current inspection of cracks under installed fasteners," *Materials Evaluation*, vol. 46, pp. 51–59, January 1991.

[3] C. V. Dodd, W. E. Deeds, and L. D. Chitwood, "Eddy current inspection of ferromagnetic materials using pulsed magnetic saturation," *Mater. Eval.*, vol. 46, pp. 1592–1597, Nov. 1988.

[4] B. Lebrun, Y. Jayet, and J.-C. Baboux, "Pulsed eddy-current signal analysis: Application to the experimental detection and characterization of deep flaws in highly conductive materials," *NDT&E Int.*, vol. 30, no. 3, pp. 163–170, 1997.

[5] R. C. Popa and K. Miya, "Approximate inverse mapping in ECT, based on aperture shifting and neural network regression," *J. Nondestr. Eval.*, vol. 17, no. 4, pp. 209–221, 1998.

[6] I. F. Hantila, G. Preda, and M. Vasiliu, "Polarization method for static fields," *IEEE Trans. Magn.*, vol. 36, pp. 672–675, July 2000.

[7] S. Kurtz, J. Fetzer, and G. Lehner, "A novel iterative algorithm for the nonlinear BEM–FEM coupling method," *IEEE Trans. Magn.*, vol. 33, pp. 1772–1775, Mar. 1997.

[8] Z. Chen and K. Miya, "ECT inversion using a knowledge-based forward solver," *J. Nondestr. Eval.*, vol. 17, no. 3, pp. 167–175, 1998.

[9] O. Mihalache, G. Preda, T. Uchimoto, K. Demachi, and K. Miya *et al.*, "Crack reconstruction in ferromagnetic materials using nonlinear FEM–BEM scheme and neural networks," in *Electromagnetic Nondestructive Evaluation (V)*, J. Pavo *et al.*, Eds. Amsterdam, The Netherlands: IOS Press, 2001, pp. 67–74.

[10] C. L. P. Chen, "A rapid supervised learning neural network for function interpolation and approximation," *IEEE Trans. Neural Networks*, vol. 7, pp. 1220–1230, Sept. 1996.